Journal of Medicinal Chemistry

Article

pubs.acs.org/jmc

Liposomal Bortezomib Nanoparticles via Boronic Ester Prodrug Formulation for Improved Therapeutic Efficacy in Vivo

Jonathan D. Ashley,[†] Jared F. Stefanick,[†] Valerie A. Schroeder,[‡,§] Mark A. Suckow,[‡,§] Tanyel Kiziltepe,*[,†,∥] and Basar Bilgicer*[,†,∥,⊥]

[†]Department of Chemical and Biomolecular Engineering, University of Notre Dame, Notre Dame, 182 Fitzpatrick Hall, Indiana 46556, United States

[‡]Department of Biological Sciences, University of Notre Dame, Notre Dame, Indiana 46556, United States

[§]Freimann Life Science Center, University of Notre Dame, Notre Dame, Indiana 46556, United States

[∥]Advanced Diagnostics and Therapeutics, University of Notre Dame, Notre Dame, Indiana 46556, United States

[⊥]Department of Chemistry and Biochemistry, University of Notre Dame, Notre Dame, Indiana 46556, United States

Supporting Information

ABSTRACT: In this study, we describe the development of liposomal bortezomib nanoparticles, which was accomplished by synthesizing bortezomib prodrugs with reversible boronic ester bonds and then incorporating the resulting prodrugs into the nanoparticles via surface conjugation. Initially, several prodrug candidates were screened based upon boronic ester stability using isobutylboronic acid as a model boronic acid compound. The two most stable candidates were then selected to create surface conjugated bortezomib prodrugs on the liposomes. Our strategy yielded stable liposomal bortezomib nanoparticles with a narrow size range of 100 nm and with high reproducibility. These liposomal bortezomib nanoparticles demonstrated significant proteasome inhibition and cytotoxicity against multiple myeloma cell lines in vitro and remarkable tumor growth inhibition with reduced systemic toxicity compared to free bortezomib in vivo. Taken together, this study demonstrates the incorporation of bortezomib into liposomal nanoparticles via reversible boronic ester bond formation to enhance the therapeutic index for improved patient outcome.

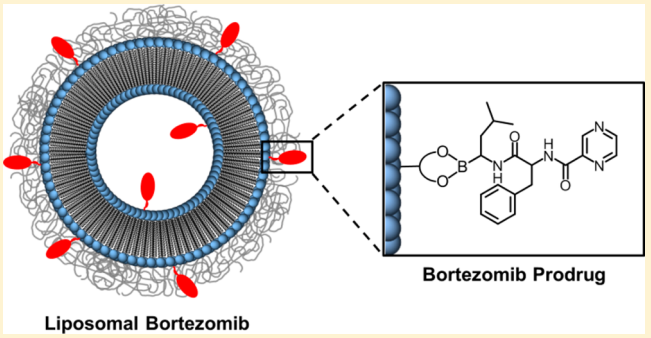

INTRODUCTION

To develop more effective treatments for cancer, studies have focused on the identification of key pathways and proteins responsible for the survival and progression of malignant cells. One target that has gained much attention over the past decade is the proteasome.[1−5] Proteasomes are intracellular proteins responsible for the degradation of damaged or misfolded proteins as well as the systematic degradation of regulatory proteins associated with cell cycle progression, cell growth, cell survival, gene expression, and stress response.[2,4,6−8] Disruption of this pathway increases the accumulation of pro-apoptotic proteins, cyclins, and cyclin-dependent kinase inhibitors while decreasing NF-κB activity within tumor cells, ultimately resulting in cell cycle arrest and apoptosis.[4,8−10] Because malignant cells exhibit a greater sensitivity to disruptions in proteasome activity when compared to healthy cells, proteasomes can be used as a viable therapeutic target for the treatment of cancers.[5,9,11] Bortezomib, a dipeptide boronic acid analogue, was the first proteasome inhibitor approved by the FDA for the treatment of cancers, specifically multiple myeloma (MM) and mantle cell lymphoma, and remains one of the most potent proteasome inhibitors available. Bortezomib inhibits proteasome activity by binding with high affinity to the catalytic sites of the 20S proteasome, particularly the chymotrypsin site, physically blocking the enzymatic activity and preventing proteolytic cleavage.[12] Although bortezomib has proven to be an effective treatment for several cancers, the dose limiting side effects, particularly peripheral neuropathy and thrombocytopenia, have inhibited it from reaching its true therapeutic potential in a broader patient population.[13−16]

In recent years, nanoparticle-based drug delivery systems have gained remarkable interest as they have greatly improved the efficacy of traditional therapeutics while decreasing the associated systemic toxicities. Nanoparticles with a diameter of 20−200 nm can selectively target and preferentially home at the tumor site via the enhanced permeability and retention (EPR) effect, a phenomenon that arises from the angiogenic blood vessels present in the tumor microenvironment which is not found in healthy endothelia.[17,18] Numerous studies have shown that nanoparticle-based therapies selectively deliver therapeutics to tumor cells which results in the decreased systemic toxicity

Received: March 5, 2014

   dx.doi.org/10.1021/jm500352v | J. Med. Chem. XXXX, XXX, XXX−XXX

associated with the off-target activity of the therapeutic agent.[19−22] Therefore, nanoparticles present ideal drug delivery vehicles for therapeutics such as bortezomib in an attempt to reduce the associated dose limiting side effects while enhancing its efficacy to improve the overall patient outcome.

While many nanoparticle formulations exist, poly(ethylene glycol) (PEG) coated liposomes are an attractive choice for use as pharmaceutical nanocarriers due to their ability to evade detection by the immune system, ease of preparation, high drug loading capabilities, and biocompatibility.[23−25] Various chemotherapeutics such as doxorubicin, cisplatin, irinotecan, and others have previously been incorporated in liposomes, demonstrating an improved therapeutic index relative to free drug.[22,26,27] In the liposomal drugs developed to date, the therapeutic agents have been predominately loaded in the aqueous core exhibiting high drug to lipid ratios.[27] However, due to the relatively poor water solubility of bortezomib, selective isolation in the aqueous core of the liposomes could significantly limit the drug loading of the particle. A viable option for incorporating bortezomib into liposomes is the direct conjugation of bortezomib to the surface of liposomes via a reversible boronic ester linkage.

In this study, we describe the development of liposomal bortezomib nanoparticles, which was accomplished by synthesizing bortezomib prodrugs with reversible boronic ester bonds and then incorporating the resulting prodrugs into liposomal nanoparticles via surface conjugation. Our results demonstrated that the liposomal bortezomib nanoparticles inhibited proteasome activity, were cytotoxic to cancer cells in vitro, and showed enhanced tumor growth inhibition with reduced systemic toxicity in vivo. Taken together, this study demonstrates the synthesis and incorporation of bortezomib prodrugs into liposomal nanoparticles to produce first-generation liposomal bortezomib nanoparticles which have enhanced therapeutic index with the long-term goal of improving patient outcome in cancers.

RESULTS

Synthesis and Evaluation of the Boronic Ester Bond Stability. Bortezomib contains a boronic acid moiety, which plays a major role in its ability to inhibit proteasome activity.[11,28] Boronic acids are known to form boronic esters with alcohols, diols, and carboxylic acid containing molecules (linkage molecules) through a reversible reaction, which can yield an unmodified boronic acid upon hydrolysis (Figure 1).[29,30] The stability of these boronic esters is known to be

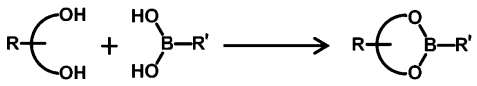

Figure 1. Schematic of the formation of boronic esters.

dependent upon the chemical structures present around the boronic ester bond.[29,31] For example, an unhindered cyclic boronic ester made from ethylene glycol is less stable and therefore hydrolyzes more rapidly than a boronic ester made from a diol with a bulky side group that sterically inhibits hydrolysis such as pinanediol.[30−33] Thus, liposomal bortezomib nanoparticles can be prepared by functionalizing liposomes with diols or a similarly reactive moiety, which can then be used to conjugate bortezomib to the liposome surface via a reversible boronic ester bond to provide controlled drug release. Moreover, the reversibility of this conjugation strategy ensures that the therapeutic is not chemically altered and that free bortezomib is released upon hydrolysis and maintains its activity.

To create a bortezomib prodrug with favorable release kinetics, the stability of the different boronic esters needs to be evaluated. Using bortezomib to evaluate the stability of the various boronic esters formed when conjugated to different linkage molecules is not a practical approach, primarily due to the large quantities of bortezomib required for each synthesis and the associated prohibitive cost. Instead, in previous studies, phenylboronic acid (PBA) was frequently used as a model compound to investigate boronic ester hydrolysis.[33−35] In these studies, PBA was conjugated to various diol-like functionalities to evaluate the stability and pH sensitivity of different PBA boronic ester bonds.[33−35] It is known that PBA, which is an aryl boronic acid, forms more stable boronic esters than alkyl boronic acids such as bortezomib at physiological pH due to the lack of an electron withdrawing group adjacent to the boronic acid.[29,36] Therefore, while the studies performed with PBA have provided insight into conjugation strategies and hydrolysis trends associated with boronic acid containing molecules, the information gained from these studies cannot be directly applied to bortezomib due to the differences in chemical properties. Instead, isobutylboronic acid (IBBA), which is an alkyl boronic acid with a similar chemical structure around the boronic acid as bortezomib, provides a better model compound to evaluate different boronic ester stabilities for nanoparticle-based bortezomib drug delivery (Figure 2a). Thus, we used IBBA as a model boronic acid to identify a linkage molecule that forms a boronic ester conjugate with optimal stability for drug delivery applications.

To investigate the stabilities of various boronic esters using IBBA as a model compound, several different compounds containing different carboxyl, hydroxyl, and amine functionalities were selected as linkage molecules to form boronic esters with IBBA (Figure 2b; **1**−**6**). Iminodiacetic acid (**1**) was shown to form very stable boronic esters in several studies and can be easily modified for nanoparticle functionalization.[37,38] Thus, it was selected as a candidate for this application. One possible caveat of **1** is that it may form boronic esters that are too stable, which would not release bortezomib from the nanoparticle and render the formulation ineffective. In that case, the carboxyl groups in **1** can be replaced with hydroxyl groups to reduce the stability of the bond while maintaining the dative bond between the boron and nitrogen atoms. Thus, linkage molecules **2** and **3** were also chosen as candidates to identify the optimal rate of hydrolysis for drug delivery. Given that the carboxyl groups significantly contribute to the stability of boronic esters, other molecules containing carboxyl groups were also selected for evaluation. Methyl salicylic acid (**4**), a derivative of salicylic acid, contains a carboxyl that is adjacent to a hydroxyl group on a phenyl ring, which provides a structure that could help stabilize the boronic ester. In addition, salicylic acid is the precursor to salicylhydroxamic acid which was shown to form boronic esters with PBA in a pH sensitive manner.[39,40] Therefore, methyl salicylhydroxamic acid (**5**) was also selected for this study. Lastly, to evaluate the effect of dative bond formation in stability, citric acid (**6**) was selected as a candidate because it can adopt similar boronic ester configurations to **1** without the presence of the dative bond to reduce the stability and facilitate drug release.

dx.doi.org/10.1021/jm500352v | J. Med. Chem. XXXX, XXX, XXX−XXX

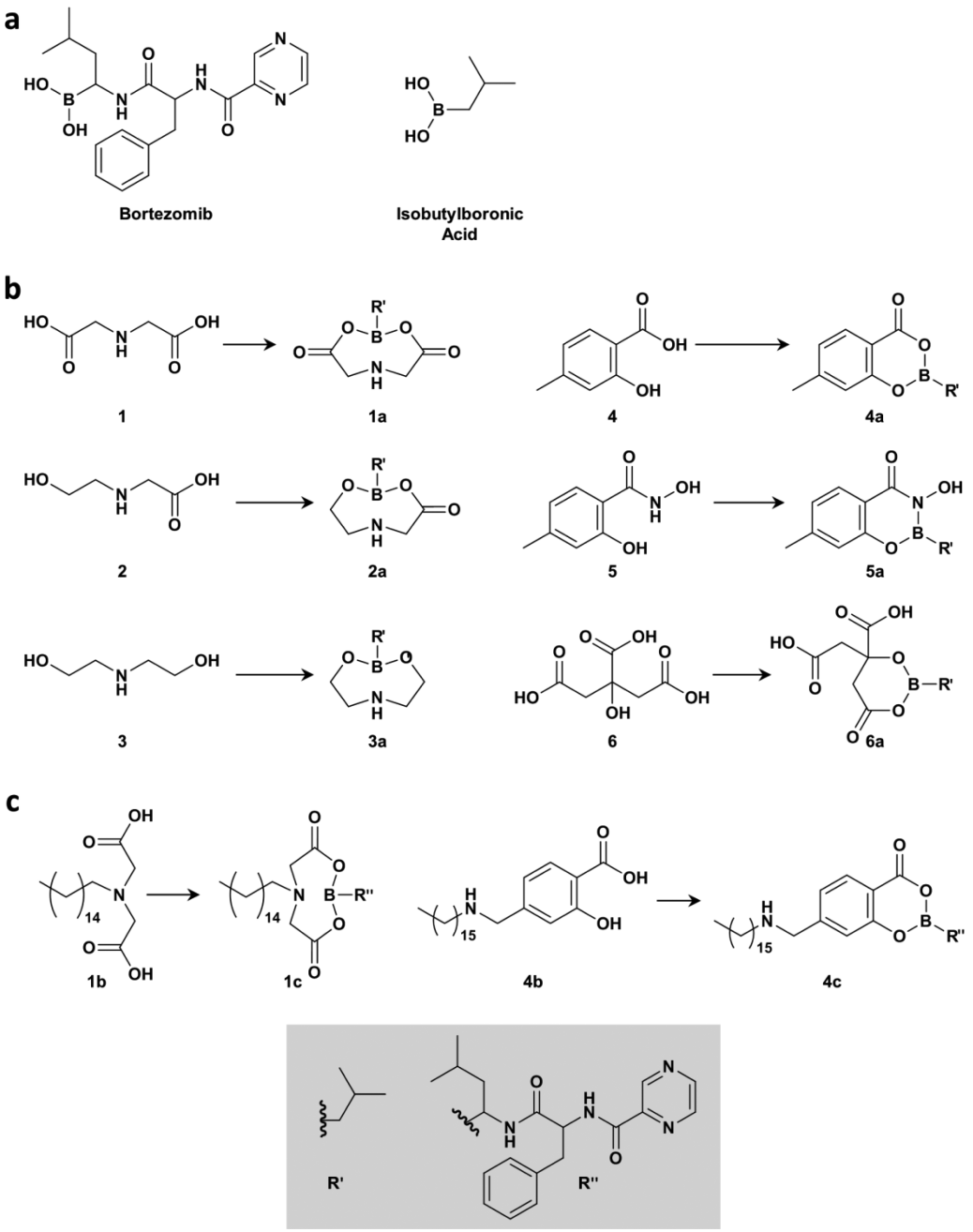

Figure 2. Linkage molecules screened for the synthesis of bortezomib prodrugs with reversible boronic ester bonds. (a) Structures of bortezomib (left) and isobutylboronic acid (right). (b) Linkage molecules (**1**–**6**) were coupled to IBBA to form the boronic ester conjugates, **1a**–**6a**, and were evaluated for the relative boronic ester stability. (c) Linkage molecules **1** and **4** were selected as promising candidates based on relative hydrolysis rates and were modified with a C_{16} aliphatic chain to yield the lipophilic molecules **1b** and **4b**, respectively. **1b** and **4b** were then used to synthesize the bortezomib prodrug conjugates **1c** and **4c**, respectively. The C_{16} aliphatic chain enabled facile insertion to the liposomes.

To evaluate the relative bond stability of the boronic esters, the model boronic acid, IBBA, was conjugated to linkage molecules **1**–**6** in toluene under refluxing conditions to generate molecules **1a**–**6a** (Figure 2b), respectively. Excess of the respective linkage molecule was used to ensure complete boronic ester formation. Post formation, each conjugate was monitored via ^{11}B NMR spectroscopy to determine hydrolysis of the boronic ester in PBS by observing the chemical shift of the boron atom as the boronic ester (~12 ppm) hydrolyzed to a boronic acid (~32 ppm) (Supporting Information Figure S1). The boronic ester formed with iminodiacetic acid (**1a**) had a half-life of $t_{1/2}$ = 190 min, which was significantly more stable than the boronic esters **2a**–**6a**. The exchange of one (**2a**) or both (**3a**) of the carboxyl groups in **1a** with a hydroxyl group significantly decreased the stability of the boronic ester conjugate, reducing the half-lives by ~21- and ~118-fold for **2a** ($t_{1/2}$ = 8.8 min) and **3a** ($t_{1/2}$ = 1.6 min), respectively, when compared to **1a**. The increased stability of **1a** over its derivatives (**2a** and **3a**) can be attributed to the strong dative bond that results from the increased acidity of the boron due to the two carboxyl groups. Methyl salicylic acid (**4**) formed the second most stable boronic ester (**4a**) with a half-life of $t_{1/2}$ = 10 min. This could be attributed to the stabilizing effects of the phenyl ring in addition to the carboxyl group. This effect was

dx.doi.org/10.1021/jm500352v | J. Med. Chem. XXXX, XXX, XXX–XXX

less pronounced with **5a** ($t_{1/2}$ = 0.4 min), where the half-life was almost 30 times shorter than **4a**. Comparing the stability of **6a** ($t_{1/2}$ = 1.6 min) to that of **1a** highlighted the significance of the dative bond in the stability of the boronic ester as **6a** lacks a central nitrogen atom to form a dative bond. The half-lives for hydrolysis for molecules **1a**–**6a** ranged from 0.4 to 190 min, and are summarized in Table 1.

Table 1. Half-Lives of Different Boronic Esters in PBS

molecule	$t_{1/2}$ (min)
1a	190 ± 45
2a	8.8 ± 0.2
3a	1.6 ± 0.4
4a	10 ± 1
5a	0.4 ± 0.1
6a	1.6 ± 0.1

It is noteworthy that although IBBA is a suitable model compound to evaluate the relative boronic ester bond stability formed with the linkage molecules (**1**–**6**) and provides a means to rank these molecules, the hydrolysis rates obtained with IBBA cannot be used as an absolute measure for bortezomib. The chemical differences between IBBA and bortezomib including the structural differences adjacent to the boronic acids between the boro-leucine in bortezomib and IBBA will alter the hydrolysis rates for bortezomib. Furthermore, bortezomib, having a phenylalanine and pyrazinoic acid moiety, possesses a more complex structure than IBBA which could impede the hydrolysis of the boronic ester, resulting in longer hydrolysis half-lives than those found using IBBA. Therefore, on the basis of the ranking information gained from the relative IBBA conjugate stabilities, linkage molecules **1** and **4** were selected as promising candidates to synthesize the bortezomib prodrugs and for their incorporation into the nanoparticles.

Synthesis of the Bortezomib Prodrugs and Formation of Liposomal Bortezomib Nanoparticles. To incorporate bortezomib into the liposomes, linkage molecules **1** and **4** were modified with a C_{16} aliphatic chain, yielding lipophilic molecules **1b** and **4b** (Figure 2c). These molecules were synthesized in such a way as not to alter the functional aspects of the molecules such that boronic esters could still be formed with bortezomib. The C_{16} tail enables the facile insertion into the bilayer of the liposomes and has a similar chain length as the other lipids used to form the liposome to maintain nanoparticle stability. Once the aliphatic modifications were made to the linkage molecules, the bortezomib prodrug conjugates **1c** and **4c** (Figure 2c) were synthesized by conjugating the lipophilic molecules **1b** and **4b**, respectively, to bortezomib via boronic ester formation by reacting in toluene under refluxing conditions for 2 h. For the formation of bortezomib prodrug incorporated nanoparticles, liposomes were first prepared without the prodrugs and extruded through a 100 nm polycarbonate membrane. Then, the prodrugs **1c** and **4c** were each postinserted into the particles with >80% efficiency (Supporting Information Figure S2) at the molar ratios of 92.5:5:2.5 DSPC:mPEG2000:Prodrug, creating the liposomal bortezomib nanoparticles NP[**1c**] and NP[**4c**], respectively (Figure 3a). The liposomal bortezomib nanoparticles yielded an average diameter of ∼100 nm based on dynamic light scattering analysis (Figure 3b), which suggested that the incorporation of the prodrugs did not alter the size of the liposomes when compared to the nondrug loaded liposomes. As an alternative approach, prodrug analogues of **1c** and **4c** without the aliphatic chains were also synthesized and incorporated into liposomal bilayer. Their encapsulation efficiencies, however, were very low with 3.8% and 11.8%, respectively, providing the rationale for the aliphatic modification for efficient drug loading.

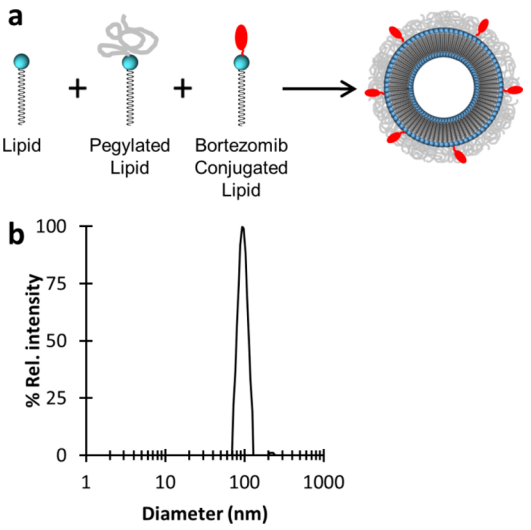

Figure 3. Preparation and characterization of liposomal bortezomib nanoparticles. (a) Illustration of the preparation of liposomal bortezomib nanoparticles. (b) Dynamic light scattering analysis revealed an average size distribution of ∼100 nm for all nanoparticles.

Liposomal Bortezomib Nanoparticles Inhibit Proteasome Activity of MM Cells and Induce Apoptosis. Once the nanoparticles were formed, proteasome inhibition assays were performed to evaluate the potency of the liposomal bortezomib nanoparticles, NP[**1c**] and NP[**4c**], to arrest proteasome activity. MM.1S and NCI-H929 MM cell lines were incubated with 25 nM bortezomib equivalent concentrations of NP[**1c**], NP[**4c**], and free bortezomib for 1, 4, and 8 h, before assessing proteasome activity (Figure 4a). At 1 h, NP[**1c**] had increased proteasome activity compared to free bortezomib and NP[**4c**]. However, at 4 and 8 h free bortezomib, NP[**1c**], and NP[**4c**] all effectively inhibited proteasome activity. The kinetic delay observed with NP[**1c**] in inhibition of proteasome activity can be attributed to the boronic ester bond stability of the **1c** bortezomib prodrug, and is in accordance with the expected differences based on hydrolysis rates obtained with the IBBA model molecule (Table 1).

After assessing proteasome activity, we evaluated if the proteasome inhibition by the liposomal bortezomib nanoparticles induced apoptosis by observing the early apoptotic marker, annexin V. MM.1S and NCI-H929 cells were incubated with 12.5 nM of equivalent bortezomib concentrations of NP[**1c**], NP[**4c**], and free bortezomib for 12 h (Figure 4b). Both nanoparticles NP[**1c**], and NP[**4c**] induced apoptosis similar to free bortezomib. Taken together, these results demonstrated that the liposomal nanoparticles NP[**1c**] and NP[**4c**] inhibited proteasome activity and induced apoptosis in MM cells similar to free bortezomib.

Liposomal Bortezomib Nanoparticles Are Cytotoxic to MM Cells. Next, we evaluated the cytotoxicity of liposomal bortezomib nanoparticles against MM cells. For this, MM.1S and NCI-H929 cells were incubated with NP[**1c**], NP[**4c**], or free bortezomib for 48 h, and cell viability was assayed by Cell

dx.doi.org/10.1021/jm500352v | J. Med. Chem. XXXX, XXX, XXX–XXX

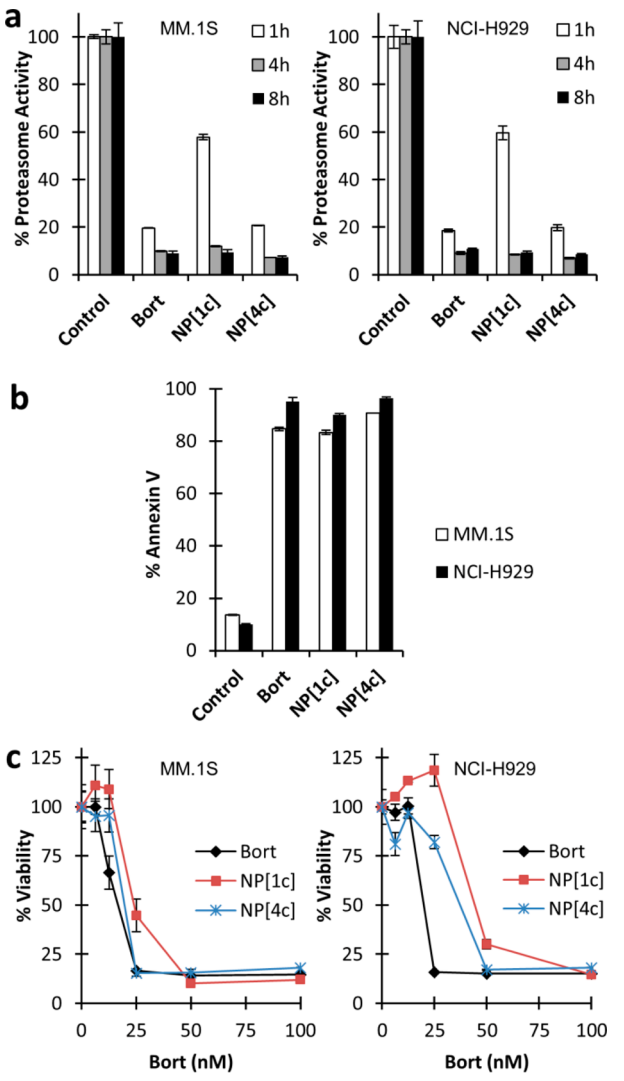

Figure 4. Liposomal bortezomib nanoparticles inhibit proteasome activity and induce apoptosis in MM cells. (a) The effect of NP[**1c**] and NP[**4c**] on proteasome inhibition was analyzed by using MM.1S and NCI-H929 MM cells. Cells were cultured in the presence of the 25 nM bortezomib equivalent concentrations of NP[**1c**], NP[**4c**], and free bortezomib for 1, 4, and 8 h. Proteasome activity was assessed using 20S Proteasome Activity Assay Kit. (b) Apoptosis was assessed by flow cytometry following Annexin-V staining at 12 h. (c) Cytotoxicity of NP[**1c**], NP[**4c**],and free bortezomib was assessed at 48 by using Cell Counting Kit-8. All data represents means (±sd) of triplicate cultures.

Counting Kit-8 reagent (Figure 4c). For MM.1S and NCI-H929 cell lines, free bortezomib had IC_{50} values of ~17 and 20 nM, respectively. The liposomal nanoparticles demonstrated slightly reduced cytotoxic effects to both MM.1S and NCI-H929 cells compared to free bortezomib, with NP[**1c**] having IC_{50} values of 25 and 45 nM, respectively, while NP[**4c**] had IC_{50} values of ~20 and 37 nM, respectively. The minor differences in the IC_{50} values between free bortezomib and the nanoparticles could be attributed to the kinetics of bortezomib release from the nanoparticles. In addition, the differences of cellular uptake pathways can also contribute to the observed differences. While free drugs enter the cells via passive diffusion, nanoparticles are taken up by endocytosis, which can result in kinetic delays in drug uptake. Taken together, these results demonstrated that the liposomal bortezomib nanoparticles were remarkably cytotoxicity against MM cells. Importantly, although NP[**1c**] and NP[**4c**] demonstrated similar cytotoxicity to free bortezomib in vitro, they have the potential to further enhance efficacy in vivo due to preferential accumulation in the tumor site via the EPR effect as has been previously observed for other therapeutics.[22,24] In addition, the esterases and acidic conditions present in the tumor microenvironment could further enhance the antitumor efficacy of NP[**1c**] and NP[**4c**] by facilitating the drug release from the particles at the tumor site.

Liposomal Nanoparticles Are Taken up by MM Cell Lines. To evaluate if liposomal nanoparticles were taken up by MM cells, fluorescein labeled liposomes were prepared and incubated with MM.1S and NCI-H929 cells for 24 h. The intracellular endocytic vesicles were stained with LyosTracker Red, the cells were fixed with 4% paraformaldehyde, and the nuclei were stained with Hoechst dye, respectively. Confocal images were collected along the *z*-axis. Our results demonstrated that the liposomes were efficiently internalized by MM cells (Figure 5). Moreover, the fluorescein signal colocalized with the LysoTracker Red signal indicating that the liposomes resided within endocytic vesicles. Control experiments performed in the absence of liposomes did not exhibit any fluorescein fluorescence.

Liposomal Bortezomib Nanoparticles Inhibit Tumor Growth and Reduce Systemic Toxicity in Vivo. An important property associated with nanoparticles is the preferential accumulation in the tumor due to the EPR effect, which reduces nonspecific toxicities associated with the free drug. Thus, the cytotoxicity observed in vitro with the liposomal bortezomib nanoparticles suggests the potential for improved efficacy in vivo. To evaluate the in vivo therapeutic potential of the liposomal bortezomib nanoparticles, CB-17 SCID mice were injected subcutaneously with NCI-H929 cells. When the tumors reached a volume of 100 mm^3, mice were randomized into treatment groups and injected with PBS, free bortezomib, NP[**1c**], or NP[**4c**] at a dose of 1 mg/kg bortezomib equivalent concentration on days 1, 4, 8, and 11. Mice were analyzed for tumor growth inhibition and systemic toxic effects. Our results indicated that both bortezomib nanoparticles NP[**1c**] and NP[**4c**] were very efficacious in tumor growth inhibition (Figure 6a). In addition, both NP[**1c**] and NP[**4c**] nanoparticles significantly improved the systemic toxicity profiles. Both nanoparticles resulted in only <10% loss in body mass during the 2 week study period, whereas the free bortezomib group demonstrated >20% weight loss and moribundity on day 7 and was consequently sacrificed due to clinical decline (Figure 6b). This improved overall systemic toxicity profile of the liposomal nanoparticles when compared to the free drug is most likely due to the EPR effect and the selective release at the tumor site. In a separate experiment, we injected tumor bearing mice with 1 mg/kg bortezomib equivalents of NP[**1c**], NP[**4c**], or free bortezomib on days 1 and 4 and sacrificed on day 5 for ex vivo analyses. Ex vivo proteasome inhibition studies demonstrated that both NP[**1c**] and NP[**4c**] demonstrated significant inhibition of proteasome activity of the tumor (Figure 6c) and induced apoptosis via caspase-3 activation (Figure 6d).

Given the relatively faster hydrolysis rate observed for linkage molecule **4** used to generate NP[**4c**] (Table 1), it is surprising but not unexpected that NP[**4c**] also demonstrated improved systemic toxicity. It is noteworthy that serum albumin has been shown to stabilize ester bonds in different therapeutics in

dx.doi.org/10.1021/jm500352v | J. Med. Chem. XXXX, XXX, XXX−XXX

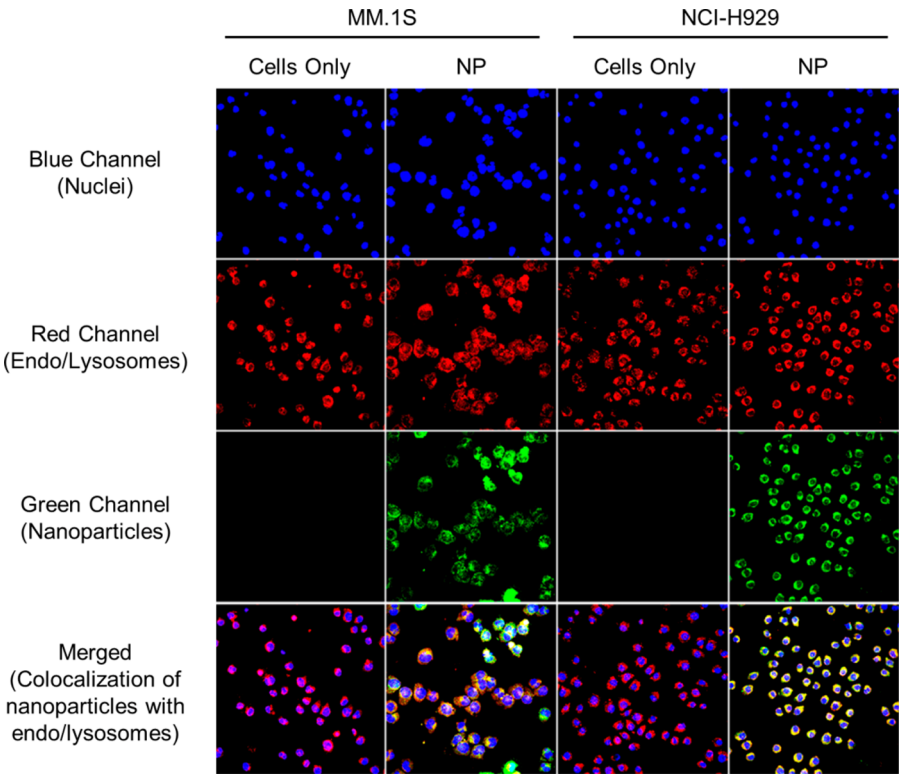

Figure 5. Cellular uptake of fluorescein labeled liposomes in MM.1S and NCI-H929 MM cell lines. MM.1S and NCI-H929 cells were incubated with fluorescein labeled liposomal nanoparticles for 24 h. Nuclei were labeled with Hoechst dye, and endosomes were labeled with LysoTracker Red. Images were taken with a Nikon A1R confocal microscope with a 40× oil lens. Image acquisition was performed by Nikon Elements Ar software.

serum.[41] This effect likely also plays a role in the boronic ester bond stability. This suggests that despite the relatively rapid hydrolysis when compared to **1c**, **4c** is stabilized long enough to reach the tumor before releasing active drug. Taken together, these results demonstrate improved efficacy and decreased systemic toxicity for liposomal bortezomib nanoparticles NP[**1c**] and NP[**4c**] when compared to free bortezomib.

DISCUSSION AND CONCLUSION

In this study, we describe the synthesis, characterization, and incorporation of bortezomib prodrug conjugates into liposomes for optimal drug delivery of bortezomib to tumors and improved therapeutic efficacy. The boronic acid moiety of bortezomib plays a major role in the proteasome inhibitory properties of the therapeutic by forming a complex with the threonine residue in the chymotrypsin-like site of the 20S proteasome. Boronic acids are known to form boronic esters with diols or diol-like moieties which can be used to sequester therapeutics containing boronic acids through the formation of reversible boronic ester bonds.[29,30] However, boronic esters are susceptible to hydrolysis and their instability poses a significant challenge in the synthesis of such prodrugs, particularly with boronic esters involving alkyl boronic acids such as bortezomib.[29,31] Therefore, in our approach, by using IBBA as a model compound, we first performed a thorough screen of several different linkage molecules with various functional groups to determine promising candidates that would yield boronic ester bonds suitable for the synthesis of bortezomib prodrugs based upon their relative stabilities. Among these, linkage molecules **1** and **4** yielded the most stable bond with IBBA with $t_{1/2}$ of 190 and 10 min, respectively. It is noteworthy that while the hydrolysis rate of **4** appears relatively fast for a controlled release application, IBBA was used only as a model compound to rank the stabilities of the different boronic esters and the absolute hydrolysis rates using bortezomib will likely be slower due to its more complex structure. Thus, we chose both **1** and **4** as promising candidates for the synthesis of bortezomib prodrugs for further evaluation. For nanoparticle preparation, aliphatically modified linkage molecules **1b** and **4b** were conjugated to bortezomib to create the boronic ester prodrugs which were then incorporated into nanoparticles to generate NP[**1c**] and NP[**4c**].

In our approach, we used PEGylated liposomes to prepare bortezomib loaded nanoparticles because of the significant advantages they provide including biocompatibility, particle size control, high drug loading capacities, and facile incorporation of different functionalities.[23−25] In addition, liposomes have been previously used in other therapeutic applications with remarkable clinical success.[27] In previous clinical applications of liposomal drug delivery systems, therapeutics were commonly encapsulated within the aqueous interior and exhibited high drug-to-lipid ratios while maintaining particle stability.[27] In our design, given the hydrophobic nature of bortezomib, we have loaded the bortezomib prodrugs onto the liposomes via a surface conjugation strategy. Therefore, in our liposomal nanoparticles, the drug loading of bortezomib directly correlated to its surface density. While this approach provided advantages such as controlled release and improved solubility, it also posed a challenge for drug loading and particle stability. Although high drug loading is desirable, the increased bortezomib density could result in the reduction of nanoparticle stealth due to steric disruptions in PEG coating. To prevent this problem, we used 5 mol % PEG2000 in our liposome formulations as was previously determined to provide

dx.doi.org/10.1021/jm500352v | J. Med. Chem. XXXX, XXX, XXX−XXX

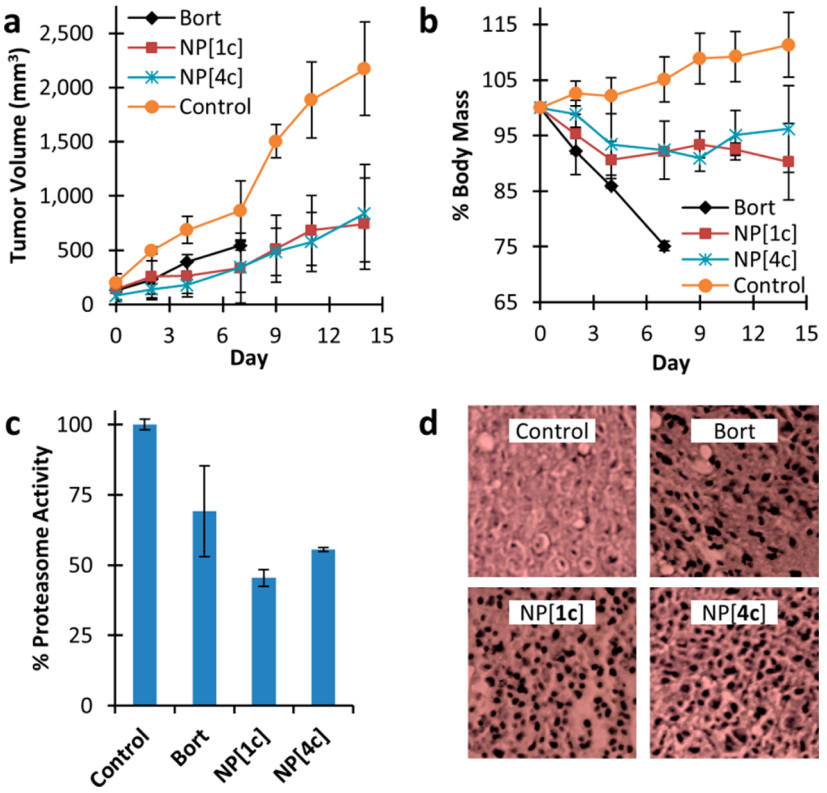

Figure 6. In vivo characterization of liposomal bortezomib nanoparticles in a xenograft multiple myeloma model. Tumor bearing SCID mice were injected, intravenously, on days 1, 4, 8, and 11, with 1 mg/kg bortezomib equivalent doses of NP[**1c**], NP[**4c**], and free bortemozib. (a) Tumor growth inhibition was detected by caliper measurements. All of the mice in the free bortezomib group were sacrificed on day 7 due to high systemic toxicity (>20% body mass). Data shown are means (±sd) of $n = 6–8$ mice per treatment group. (b) Percentage of body weight of the animals was used as an indication of systemic toxicity. The free bortezomib group significantly lost body mass (>20%) and showed moribundity by day 7 and was therefore sacrificed. Only <10% weight loss was observed with NP[**1c**] and NP[**4c**] during this study. (c) Ex vivo proteasome inhibition assay of excised tumors. Four additional mice per group were injected on days 1 and 4 with a dose of 1 mg/kg bortezomib equivalent concentrations. Mice were sacrificed 24 h after treatment, and tumors were analyzed for proteasome inhibition. (d) Ex vivo mechanistic analysis of the tumors for apoptosis. Excised tumors were stained for activated caspase-3. Representative images of the tumor cross sections obtained using a Nikon Eclipse TS100 microscope at ×20 magnification are shown.

optimal stealth and maintained the drug loading below 5 mol % to avoid PEG crowding in order to maintain the stability of the liposomes.[42,43] Thus, a prodrug loading of 2.5 mol % was selected for the preparation of liposomal bortezomib nanoparticles, which yielded stable liposomes with high reproducibility and a narrow size range of 100 nm. Ongoing studies in our lab are investigating methods to further increase the nanoparticle drug loading without compromising particle stability.

While this study focuses solely on the synthesis of bortezomib prodrugs for nanoparticle incorporation, the strategies developed within this report can also be applied to other therapeutic or diagnostic molecules containing a boronic acid moiety including serine protease inhibitors, boron neutron capture therapeutic agents, and other proteasome inhibitors for improved targeting and efficacy. Importantly, the strategies described in this study for the incorporation of bortezomib into nanoparticles are not limited to liposomes but can be applied to other types of nanoparticles such as polymeric nanoparticles, gold nanoparticles, dendrimers, or micelles. Hence, this methodology establishes a platform that utilizes boronic ester chemistry to facilitate the incorporation of boronic acid containing molecules into various nanoparticle-based drug delivery systems for improved diagnostic and therapeutic outcomes.

In preclinical evaluation of the liposomal bortezomib nanoparticles, both NP[**1c**] and NP[**4c**] demonstrated significant proteasome inhibition, induced apoptosis, and cytotoxicity in MM cells in vitro and dramatically reduced the nonspecific toxicities associated with free bortezomib while maintaining significant tumor growth inhibition in vivo. These studies demonstrated that, despite being an effective chemotherapeutic, the therapeutic efficacy of bortezomib can be further improved by utilizing the enhanced tumor accumulation properties afforded by nanoparticle-based drug delivery systems to reduce nonspecific toxicities. In an ongoing study in our lab, we are developing quantitative analytical methods to accurately determine bortezomib concentration in tissues in order to perform a thorough in vivo biodistribution study with liposomal bortezomib. In this study, we have shown that the improved therapeutic index and reduced systemic toxicity profile associated with the liposomal bortezomib nanoparticles demonstrates their potential to overcome the adverse events associated with bortezomib in the clinic such that a broader patient population can benefit from this effective therapeutic. Taken together, this study provides the preclinical rationale for the clinical evaluation of liposomal bortezomib nanoparticles for improved patient outcome in cancers.

dx.doi.org/10.1021/jm500352v | J. Med. Chem. XXXX, XXX, XXX–XXX

EXPERIMENTAL SECTION

Reagents. The membranes (0.1 μm), mini-extruder, and all lipid components were purchased from Avanti Polar Lipids, Inc. (Alabaster, AL). Bortezomib was purchased from GenDepot (Barker, TX). All other chemicals, including molecules **1**, **3**, **4**, and **6**, were purchased from Sigma-Aldrich and were reagent grade or better (St. Louis, MO). Purity of titled compounds was determined via either HPLC or ^{1}H NMR and were tested to be >95% pure. High resolution mass spectrometry (HRMS) analysis was performed on a Bruker Q-TOF system.

Synthesis of 2-((2-Hydroxyethyl)amino)acetic Acid [2]. First, 2 mmol of ethanolamine and 2 mmol of diisopropylethylamine (DIPEA) were mixed in 30 mL of methanol in a flame-dried 200 mL round-bottom flask. Then 2 mmol of methyl bromoacetate was added dropwise over a period of 1 min into the solution while stirring. The reaction proceeded under reflux overnight while stirring. The solution was cooled to room temperature, and the solvent was removed under vacuum. The solids were dissolved in 1.3 mL of EtOH and diluted into 6 mL of 1 M NaOH. The solution was heated to reflux for 1 h. The pH of the solution was then adjusted to 7 with 10 M HCl and evaporated to dryness. ^{1}H NMR (400 MHz, D_2O) δ 4.24 (s, 1H), 4.00 (s, 1H), 3.87 (s, 2H), 3.81 (t, 2H), 3.13 (t, 2H). ESI HRMS for $C_4H_9NO_3$: calculated m/z 120.0655 $[M + H]^+$; found 120.0691.

Synthesis of *N*,2-Dihydroxy-4-methylbenzamide [5]. First, 252.5 mg of 4-methylsalicylic acid (1.66 mmol) was dissolved with 20 mL of MeOH in a 50 mL round-bottom flask. Then 0.5 mL of 18 M sulfuric acid was added while stirring. The reaction proceeded under reflux for 24 h while stirring. The reaction was quenched by adding 100 mL of water to the solution. The intermediate was extracted with ethyl ether (3 × 30 mL). The organic phases were combined and washed with a saturated sodium bicarbonate solution (2 × 100 mL). The ether was evaporated in vacuo, and the intermediate was dissolved in 0.5 mL of THF. The intermediate solution was added dropwise to a $NaOH/NH_2OH$ solution (6.72 mL of 1.64 M NH_2OH in water was added to 8.38 mL of 3 M NaOH) while stirring. The reaction was allowed to proceed at room temperature for 24 h. After 24 h, the reaction was cooled to 0 °C using an ice bath, and the pH was adjusted to 5 with 10 M HCl. The solution was allowed to warm to room temperature before extracting the product with ethyl acetate (3 × 15 mL). The organic layers were combined, and the solvent was evaporated. ^{1}H NMR (400 MHz, DMSO-d_6) δ12.30 (s, 1H), 11.39 (s, 1H), 9.28 (s, 1H), 7.56 (d, J = 8.28 Hz, 1H), 6.71 (s, 1H), 6.67 (d, J = 7.89 Hz, 1H), 2.54 (s, 1H), 2.25 (s, 3H). ESI HRMS for $C_8H_9NO_3$: calculated m/z 168.0655 $[M + H]^+$; found 168.0711.

Synthesis of 2,2′-(Hexadecylazanediyl)diacetic Acid [1b]. First, 1.81 g of hexadecylamine (7.5 mmol) was dissolved in 75 mL of MeOH in a flame-dried 250 mL round-bottom flask. Then 3.92 mL of DIPEA (30 mmol) and 2.29 g of methyl bromoacetate (15 mmol) were added to the flask while stirring. The reaction proceeded under reflux for 96 h while stirring. Next, the solvent was removed under vacuum and the solids were dissolved in chloroform. The intermediate product was purified via flash chromatography using 5% methanol in chloroform solution. The solution was concentrated by rotary evaporation then diluted into 400 mL of 0.5 M NaOH. The solution was refluxed until it became clear (~2 h). The solution was then cooled to room temperature and the pH adjusted to 2 using 10 M HCl causing a white precipitate to form. The product was filtered, washed, and dried in vacuo overnight. ^{1}H NMR (500 MHz, DMSO-d_6) δ 3.41 (s, 4H), 2.62 (t, 2H), 1.23 (s, 28H), 0.85 (t, 3H). ESI HRMS for $C_{20}H_{39}NO_4$: calculated m/z 358.2952 $[M + H]^+$; found 358.2899.

Synthesis of 4-((Hexadecylamino)methyl)-2-hydroxybenzoic Acid [4b]. First, 1.521 g of methyl salicylic acid (10 mmol) was dissolved in 50 mL of MeOH in a 200 mL round-bottom flask. Then 3 mL of sulfuric acid was added to the solution. The flask was connected to a condenser (T = 5 °C) and heated to reflux for 24 h. The reaction was quenched by adding 100 mL of water to the solution. The intermediate was extracted with ethyl ether (3 × 50 mL). The organic phases were combined and washed with a saturated sodium bicarbonate solution (2 × 100 mL). The ether was evaporated in vacuo and the intermediate was dissolved in 40 mL of carbon tetrachloride. Then 2.225 g of *N*-bromosuccinimide (12.5 mmol) and 0.726 g of benzoyl peroxide (3 mmol) were added to the solution. The solution was refluxed while stirring for 4 h. The brominated intermediate was purified via flash chromatography using 2% methanol in chloroform solution and concentrated by rotary evaporation to a volume of 5 mL. To the concentrate solution, 2.4 g of hexadecylamine (10 mmol) and 2.5 g of DIPEA (20 mmol) in 70 mL of MeOH were added. The reaction proceeded under reflux for 24 h while stirring. After the 24 h, the solvent was removed via rotary evaporation and the solids were dissolved in chloroform. The intermediate product was purified via flash chromatography using 3% methanol in chloroform solution. The solution was concentrated by rotary evaporation then diluted into 400 mL of 0.5 M NaOH. The solution was boiled for 2 h. A white precipitate formed and the product was filtered, washed, and dried in vacuo overnight. ^{1}H NMR (400 MHz, $CDCl_3$) δ 7.42–7.81 (m, 1H), 6.57–7.01 (m, 2H), 3.67–4.16 (m, 2H), 2.76–3.20 (m, 2H), 1.53–1.88 (m, 2H), 0.97–1.44 (m, 26H), 0.87 (t, J = 6.69 Hz, 3H). ESI HRMS for $C_{24}H_{41}NO_3$: calculated m/z 392.3159 $[M + H]^+$; found 392.3116.

Synthesis of the Boronic Acid Conjugates [1a–6a, 1c, and 4c]. The linkage molecule and the boronic acid (IBBA or bortezomib) at a molar ratio of 1:1 were placed in a flame-dried 25 mL flask with 7 mL of toluene. The solution was allowed to reflux for 2 h while stirring before being removed from the heat. The solvent was then evaporated in vacuo. Conjugation was verified using ^{1}H NMR and ^{11}B NMR spectroscopy to observe the peak shift of the boron from ~32 ppm (boronic acid) to ~9 ppm (boronic ester) via Bruker AVANCE III HD 400 MHz spectrometer (Bruker, Billerica, MA).

*2-Isobutyl-1,3,6,2-dioxazaborocane-4,8-dione (**1a**).* ^{1}H NMR (400 MHz, DMSO-d_6) δ 3.90–4.09 (m, 4H), 1.63–1.74 (m, 1H), 0.90 (d, J = 6.69 Hz, 6H), 0.45 (d, J = 7.08 Hz, 2H). ESI HRMS m/z calculated for $C_8H_{14}BNO_4$: calculated m/z 200.1090 $[M + H]^+$, found 200.1077.

*N-((S)-1-(((R)-1-(6-Hexadecyl-4,8-dioxo-1,3,6,2-dioxazaborocan-2-yl)-3-methylbutyl)amino)-1-oxo-3-phenylpropan-2-yl)pyrazine-2-carboxamide (**1c**).* ^{1}H NMR (500 MHz, DMSO-d_6) δ 9.05–9.08 (m, 1H), 8.85–8.92 (m, 3H), 8.71–8.75 (m, 1H), 7.21–7.29 (m, 5H), 4.66–4.69 (m, 1H), 3.36 (s, 4H), 3.06–3.08 (m, 2H), 2.63 (t, 1H), 1.41–1.43 (m, 1H), 1.39–1.41 (m, 1H), 1.36–1.38 (m, 1H), 1.16–1.32 (m, 28H), 0.82–0.82 (m, 0H), 0.84 (t, 6H), 0.81 (t, 3H). ESI HRMS for $C_{39}H_{60}BN_5O_6$: calculated m/z 706.4735 $[M + H]^+$; found 706.4709.

*2-Isobutyl-1,3,6,2-dioxazaborocan-4-one (**2a**).* ^{1}H NMR (400 MHz, DMSO-d_6) δ 3.86 (s, 1H), 3.61–3.69 (m, 2H), 3.55 (t, J = 5.31 Hz, 2H), 2.80 (t, 2H) δ 1.74 (m, 1H), 0.78 (d, 6H), 0.48 (d, 2H). ESI HRMS for $C_8H_{16}BNO_3$: calculated m/z 186.1298 $[M + H]^+$; found 186.1300.

*2-Isobutyl-1,3,6,2-dioxazaborocane (**3a**).* ^{1}H NMR (400 MHz, DMSO-d_6) δ 6.44 (s, 1H), 3.62–3.72 (m, 2H), 3.55 (d, J = 3.54 Hz, 2H), 2.89–3.01 (m, 2H), 2.60–2.70 (m, 2H), 1.50–1.66 (m, 1H), 0.83 (d, J = 6.29 Hz, 6H), 0.18 (d, J = 6.69 Hz, 2H). ESI HRMS for $C_8H_{18}BNO_2$: calculated m/z 172.1503 $[M + H]^+$; found 172.1500.

*2-Isobutyl-7-methyl-4H-benzo[d][1,3,2]dioxaborinin-4-one (**4a**).* ^{1}H NMR (500 MHz, DMSO-d_6) δ 7.59 (d, 1H), 6.64–6.71 (m, 2H), 2.26 (s, 3H), 1.57–1.71 (m, 1H), 0.85 (d, 6H), 0.38 (d, 4H). ESI HRMS for $C_{12}H_{15}BO_3$: calculated m/z 219.1187 $[M + H]^+$; found 219.1179.

*N-((S)-1-(((R)-1-(7-(((Hexadecylamino)methyl)-4-oxo-4H-benzo-[d][1,3,2]dioxaborinin-2-yl)-3-methylbutyl)amino)-1-oxo-3-phenyl-propan-2-yl)pyrazine-2-carboxamide (**4c**).* ^{1}H NMR (400 MHz, DMSO-d_6) 9.09–9.14 (m, 1H), 8.86–8.93 (m, 2H), 8.71–8.78 (m, 2H), 7.73–7.87 (m, 5H), δ 7.19–7.32 (m, 1H), 6.84–7.10 (m, 2H), 5.00–5.14 (m, 2H), 4.06–4.21 (m, 2H), 3.12–3.18 (m, 2H), 2.85–2.94 (m, 2H), 2.53–2.55 (m, 1H), 1.45–1.65 (m, 2H), 1.39 (none, 2H), 1.23 (s, 26H), 0.78–0.88 (m, 9H). ESI HRMS for $C_{43}H_{62}BN_5O_5$: calculated m/z 740.4917 $[M + H]^+$; found 740.4927.

*3-Hydroxy-2-isobutyl-7-methyl-2,3-dihydro-4H-benzo[e][1,3,2]-oxazaborinin-4-one (**5a**).* ^{1}H NMR (300 MHz, DMSO-d_6) δ 11.38 (s, 1H), 7.56 (d, J = 8.01 Hz, 1H), 6.71 (s, 1H), 6.67 (d, 1H), 2.25 (s,

dx.doi.org/10.1021/jm500352v | J. Med. Chem. XXXX, XXX, XXX–XXX

3H), 1.69−1.86 (m, 1H), 0.85 (d, J = 6.63 Hz, 6H), 0.53 (d, J = 7.46 Hz, 2H). ESI HRMS for $C_{12}H_{16}BNO_3$: calculated m/z 234.1299 $[M + H]^+$; found 234.1335.

*4-(Carboxymethyl)-2-isobutyl-6-oxo-1,3,2-dioxaborinane-4-carboxylic Acid (**6a**).* ^{1}H NMR (400 MHz, DMSO-d_6) δ 2.57−2.65 (m, 4H), 1.58−1.72 (m, 1H), 0.84 (d, J = 6.69 Hz, 6H), 0.37 (d, J = 6.69 Hz, 2H). ESI HRMS for $C_{10}H_{15}BO_7$: calculated m/z 257.0829 $[M - H]^-$; found 257.0821.

Hydrolysis of Boronic Esters. 0.2 mmol of the boronic ester conjugates, **1a**−**6a**, were dissolved in 0.4 mL of DMSO-d_6 and divided into two 0.2 mL vials. One solution was diluted with 0.2 mL of PBS, while the other was diluted with 0.2 mL of DMSO-d_6 as a control. ^{11}B spectra were obtained at t = 0, 5, 10, and 30 min for each solution at 128 MHz using the Bruker AVANCE III HD 400 MHz spectrometer equipped with a standard 5 mm broadband probe (Bruker, Billerica, MA). The following experimental parameters were used: acquisition time 1.42 s, relaxation delay 2.0 s, 256 scans. Hydrolysis of the boronic ester was measured by observing the reduction of the peak at ∼12 ppm.

Liposome Preparation. Liposomes were prepared by dry film hydration as described previously.[44] Briefly, lipids were mixed at the indicated ratio in chloroform, dried to form a thin film using nitrogen gas, and then placed under vacuum overnight to remove residual solvent. The lipid films were hydrated at 65 °C in PBS pH 7.4 with gently agitated and extruded at 65 °C through a 0.1 μm polycarbonate filter. Liposomes all adhered to the following formula 92.5:5:2.5 DSPC:mPEG2000:Prodrug.

Particle Sizing. Dynamic light scattering analysis was performed using the 90Plus nanoparticle size analyzer (Brookhaven Instruments, Holtsville, NY) as previously described.[19]

Cell Culture. MM.1S and NCI-H929 cell lines were obtained from American Type Culture Collection (Rockville, MD). Both cell lines were supplemented with 10% fetal bovine serum (FBS), 2 mM L-glutamine (Gibco, Carlsbad, CA), 100 μg/mL penicillin, and 100 μg/mL streptomycin (Gibco). NCI-H929 cells were further supplemented with 55 μM 2-mercaptoethanol.

Cytotoxicity Assays. Cell Counting Kit-8 (Dojindo Molecular Technologies, Rockville, MD) was used as previously described.[19]

In Vitro Proteasome Inhibition Assays. 20S Proteasome Activity Assay Kit (EMD Millipore, Billerica, MA) was used to measure proteasome activity. Briefly, 6 × 10^5 cells/well were plated in a 6 well dish. NP[**1c**], NP[**4c**], or free bortezomib were added at 25 nM bortezomib equivalent concentrations to their respective wells and incubated for 1, 4, or 8 h at 37 °C. Cells were washed twice with cold PBS and lysed in 60 μL of lysis buffer (50 mM HEPES, 5 mM EDTA, 150 mM NaCl, 1% Triton X-100, pH 7.5) on ice for 30 min by periodic vortexing. The lysate was centrifuged at 21130g for 15 min at 4 °C. Then 10 μL of the lysate, along with 10 μL of proteasome substrate (Suc-LLVY-AMC) and 80 μL of the assay buffer (25 mM HEPES, pH 7.5, 0.5 mM EDTA, 0.05% NP-40, and 0.001% SDS (w/v)), was placed into a 96 well plate and incubated at 37 °C for 1 h. Proteasome activity was assessed via fluorescence spectroscopy (ex 380 nm/em 460 nm).

Flow Cytometry. Apoptotic cells were detected with Annexin-V (FITC) antibody (BD Pharmigen, Sandiego, CA). Cells were analyzed with Guava EasyCyte flow cytometer (EMD Millipore) as previously described.[19]

Confocal Microscopy. Confocal experiments were performes as previously described.[45] Briefly, 1 × 10^5 cells/well were plated 24 h prior to each experiment in a 24 well dish. Liposomes were added at 100 μM phospholipid concentration and incubated for 24 h at 37 °C. 1% DOPE-CF was added as a fluorescent marker to each liposomal formulation. Cells were washed 3 times with PBS and incubated in 50 nM LysoTracker Red (Molecular Probes, Carlsbad, CA) in culture media for 30 min at 37 °C to allow internalization. After 30 min, cells were washed 3 times with PBS and spun onto slides, using a Cytospin (Thermo Fisher Scientific, Waltham, MA) before being fixed with 4% paraformaldehyde. Slides were rinsed with PBS then incubated with 2 μg/mL Hoechst dye (Sigma-Aldrich) in PBS for 15 min to stain the nucleus. Coverslips were mounted on microscope slides with Prolong Gold Antifade (Molecular Probes). Cells were visualized with a Nikon A1R confocal microscope using a 40× oil lens (Nikon Instruments, Melville, NY). Image acquisition was performed by Nikon Elements Ar software (Nikon).

MM Xenograft Mouse Model. CB-17 SCID mice (Harlan Laboratories, Indianapolis, IN) were irradiated with 150 rad and were inoculated subcutaneously with 5 × 10^6 NCI-H929 cells. When tumors reached a volume of 100 mm^3, mice were distributed into four groups of 6−8 mice and were treated intravenously with NP[**1c**], NP[**4c**], free bortezomib, or vehicle (PBS), on days 1, 4, 8, and 11 at a dose of 1 mg/kg bortezomib equivalents. Animals were monitored for body weight and tumor volume. Tumor volume was measured via calipers (volume = 0.5 × length × $(width)^2$). Mice were treated humanely and in accordance with the protocol approved by the Institutional Animal Care and Use Committee (IACUC) at the Freimann Life Science Center (Notre Dame, IN).

Ex Vivo Proteasome Inhibition and Apoptosis Assays. CB-17 SCID mice were irradiated with 150 rad and were inoculated subcutaneously with 5 × 10^6 NCI-H929 cells. When tumors were palpable, mice were distributed into four groups of 4 mice and were treated intravenously with NP[**1c**], NP[**4c**], free bortezomib, or PBS, on days 1 and 4 at a dose of 1 mg/kg bortezomib equivalents. The mice were sacrificed on day five, and the tumors were excised and divided in half. For detection of apoptosis, one-half was fixed in formalin solution and immunohistochemical staining for caspase-3 was performed as previously described.[19] The other half was used for the proteasome inhibition assay. Tumors were homogenized in 0.2 mL of lysis buffer (100 mM Tris, pH 7.8, 150 mM NaCl, 1% Triton-X100) per 50 mg tissue. The homogenate was centrifuged at 18400g for 10 min at 4 °C. The supernatant was removed and centrifuged again to ensure complete removal of any precipitate. The protein concentration of each sample was determined using Bradford assay, and samples were diluted to a protein concentration of 15 μg/mL. 20S Proteasome Activity Assay Kit (EMD Millipore) was used to measure proteasome activity. Then 10 μL of the respective homogenate, along with 10 μL of proteasome substrate (Suc-LLVY-AMC) and 80 μL of the assay buffer (25 mM HEPES, pH 7.5, 0.5 mM EDTA, 0.05% NP-40, and 0.001% SDS (w/v)), was placed into a 96 well plate and incubated at 37 °C for 1 h. Proteasome activity was assessed via fluorescence spectroscopy (ex 380 nm/em 460 nm).

■ ASSOCIATED CONTENT

Ⓢ Supporting Information

Representative ^{11}B-NMR spectra and HLPC chromatograms of loading efficiency for the prodrugs. This material is available free of charge via the Internet at http://pubs.acs.org.

■ AUTHOR INFORMATION

Corresponding Authors

*For T.K.: phone, 574-631-1603; E-mail, tkiziltepe@nd.edu.
*For B.B.: phone, 574-631-1429; E-mail, bbilgicer@nd.edu.

Notes

The authors declare no competing financial interest.

■ ACKNOWLEDGMENTS

We thank the Notre Dame Integrated Imaging Facility for confocal microscopy, the Center for Environmental Science and Technology for the use of DLS, the Mass Spectrometry and Proteomics Facility for the use of their mass spectrometers, and the Magnetic Resonance Research Center for the use of the Bruker 400 MHz spectrometer. We thank Deborah Donahue and the W. M. Keck Center for the irradiation of the mice. We thank Sarah Chapman for preparing the histology sections. This work was supported by the Hollis Brownstein Research Program Grant from Leukemia Research Foundation.

■ ABBREVIATIONS USED

DIPEA, diisopropylethylamine; DOPE-CF, 1,2-dioleoyl-*sn*-glycero-3-phosphoethanolamine-*N*-(carboxyfluorescein); DSPC, 1,2-distearoyl-*sn*-glycero-3-phosphocholine; EPR, enhanced permeability and retention; IBBA, isobutylboronic acid; mPEG2000, 1,2-dipalmitoyl-*sn*-glycero-3-phosphoethanolamine-*N*-[methoxy(poly(ethylene glycol))-2000]; MM, multiple myeloma; PBA, phenylboronic acid

■ REFERENCES

(1) Genin, E.; Reboud-Ravaux, M.; Vidal, J. Proteasome inhibitors: recent advances and new perspectives in medicinal chemistry. *Curr. Top. Med. Chem.* **2010**, *10*, 232−256.

(2) Chauhan, D.; Hideshima, T.; Anderson, K. C. Proteasome inhibition in multiple myeloma: therapeutic implication. *Annu. Rev. Pharmacol. Toxicol.* **2005**, *45*, 465−476.

(3) Chauhan, D.; Hideshima, T.; Mitsiades, C.; Richardson, P.; Anderson, K. Proteasome inhibitor therapy in multiple myeloma. *Mol. Cancer Ther.* **2005**, *4*, 686−692.

(4) Almond, J. B.; Cohen, G. M. The proteasome: a novel target for cancer chemotherapy. *Leukemia* **2002**, *16*, 433−443.

(5) Orlowski, R. Z.; Kuhn, D. J. Proteasome inhibitors in cancer therapy: lessons from the first decade. *Clin. Cancer Res.* **2008**, *14*, 1649−1657.

(6) Hideshima, T.; Mitsiades, C.; Akiyama, M.; Hayashi, T.; Chauhan, D.; Richardson, P.; Schlossman, R.; Podar, K.; Munshi, N. C.; Mitsiades, N.; Anderson, K. C. Molecular mechanisms mediating antimyeloma activity of proteasome inhibitor PS-341. *Blood* **2003**, *101*, 1530−1534.

(7) Mitsiades, N.; Mitsiades, C. S.; Poulaki, V.; Chauhan, D.; Fanourakis, G.; Gu, X. S.; Bailey, C.; Joseph, M.; Libermann, T. A.; Treon, S. P.; Munshi, N. C.; Richardson, P. G.; Hideshima, T.; Anderson, K. C. Molecular sequelae of proteasome inhibition in human multiple myeloma cells. *Proc. Natl. Acad. Sci. U. S. A.* **2002**, *99*, 14374−14379.

(8) Hideshima, T.; Richardson, P.; Chauhan, D.; Palombella, V.; Elliott, P.; Adams, J.; Anderson, K. The proteasome inhibitor PS-341 inhibits growth, induces apoptosis, and overcomes drug resistance in human multiple myeloma cells. *Cancer Res.* **2001**, *61*, 3071−3076.

(9) Rajkumar, S.; Richardson, P.; Hideshima, T.; Anderson, K. Proteasome inhibition as a novel therapeutic target in human cancer. *J. Clin. Oncol.* **2005**, *23*, 630−639.

(10) Mitsiades, N.; Mitsiades, C.; Poulaki, V.; Chauhan, D.; Fanourakis, G.; Gu, X.; Bailey, C.; Joseph, M.; Libermann, T.; Treon, S.; Munshi, N.; Richardson, P.; Hideshima, T.; Anderson, K. Molecular sequelae of proteasome inhibition in human multiple myeloma cells. *Proc. Natl. Acad. Sci. U. S. A.* **2002**, *99*, 14374−14379.

(11) Richardson, P. G.; Hideshima, T.; Anderson, K. C. Bortezomib (PS-341): a novel, first-in-class proteasome inhibitor for the treatment of multiple myeloma and other cancers. *Cancer Control* **2003**, *10*, 361−369.

(12) Dick, L. R.; Fleming, P. E. Building on bortezomib: second-generation proteasome inhibitors as anti-cancer therapy. *Drug Discovery Today* **2010**, *15*, 243−249.

(13) Arastu-Kapur, S.; Anderl, J. L.; Kraus, M.; Parlati, F.; Shenk, K. D.; Lee, S. J.; Muchamuel, T.; Bennett, M. K.; Driessen, C.; Ball, A. J.; Kirk, C. J. Nonproteasomal targets of the proteasome inhibitors bortezomib and carfilzomib: a link to clinical adverse events. *Clin. Cancer Res.* **2011**, *17*, 2734−2743.

(14) Chen, D.; Frezza, M.; Schmitt, S.; Kanwar, J.; Dou, Q. P. Bortezomib as the first proteasome inhibitor anticancer drug: current status and future perspectives. *Curr. Cancer Drug Targets* **2011**, *11*, 239−253.

(15) Curran, M. P.; McKeage, K. Bortezomib a review of its use in patients with multiple myeloma. *Drugs* **2009**, *69*, 859−888.

(16) Bruna, J.; Ale, A.; Velasco, R.; Jaramillo, J.; Navarro, X.; Udina, E. Evaluation of pre-existing neuropathy and bortezomib retreatment as risk factors to develop severe neuropathy in a mouse model. *J. Peripher. Nerv. Syst.* **2011**, *16*, 199−212.

(17) Maeda, H.; Wu, J.; Sawa, T.; Matsumura, Y.; Hori, K. Tumor vascular permeability and the EPR effect in macromolecular therapeutics: a review. *J. Controlled Release* **2000**, *65*, 271−284.

(18) Patricia Egusquiaguirre, S.; Igartua, M.; Maria Hernandez, R.; Luis Pedraz, J. Nanoparticle delivery systems for cancer therapy: advances in clinical and preclinical research. *Clin. Transl. Oncol.* **2012**, *14*, 83−93.

(19) Kiziltepe, T.; Ashley, J. D.; Stefanick, J. F.; Qi, Y. M.; Alves, N. J.; Handlogten, M. W.; Suckow, M. A.; Navari, R. M.; Bilgicer, B. Rationally engineered nanoparticles target multiple myeloma cells, overcome cell-adhesion-mediated drug resistance, and show enhanced efficacy in vivo. *Blood Cancer J.* **2012**, *2*, e64.

(20) Allen, T. M.; Cullis, P. R. Liposomal drug delivery systems: from concept to clinical applications. *Adv. Drug Delivery Rev.* **2013**, *65*, 36−48.

(21) Paraskar, A. S.; Soni, S.; Chin, K. T.; Chaudhuri, P.; Muto, K. W.; Berkowitz, J.; Handlogten, M. W.; Alves, N. J.; Bilgicer, B.; Dinulescu, D. M.; Mashelkar, R. A.; Sengupta, S. Harnessing structure−activity relationship to engineer a cisplatin nanoparticle for enhanced antitumor efficacy. *Proc. Natl. Acad. Sci. U. S. A.* **2010**, *107*, 12435−12440.

(22) Boulikas, T. Low toxicity and anticancer activity of a novel liposomal cisplatin (Lipoplatin) in mouse xenografts. *Oncol. Rep.* **2004**, *12*, 3−12.

(23) Gabizon, A.; Catane, R.; Uziely, B.; Kaufman, B.; Safra, T.; Cohen, R.; Martin, F.; Huang, A.; Barenholz, Y. Prolonged circulation time and enhanced accumulation in malignant exudates of doxorubicin encapsulated in polyethylene-glycol coated liposomes. *Cancer Res.* **1994**, *54*, 987−992.

(24) Allen, T. M.; Cheng, W. W. K.; Hare, J. I.; Laginha, K. M. Pharmacokinetics and pharmacodynamics of lipidic nano-particles in cancer. *Anti-Cancer Agents Med. Chem.* **2006**, *6*, 513−523.

(25) Allen, T. Liposomal drug formulations—rationale for development and what we can expect for the future. *Drugs* **1998**, *56*, 747−756.

(26) Barenholz, Y. Doxil—The first FDA-approved nano-drug: lessons learned. *J. Controlled Release* **2012**, *160*, 117−134.

(27) Chang, H.; Yeh, M. Clinical development of liposome-based drugs: formulation, characterization, and therapeutic efficacy. *Int. J. Nanomed.* **2012**, *7*, 49−60.

(28) Trippier, P. C.; McGuigan, C. Boronic acids in medicinal chemistry: anticancer, antibacterial and antiviral applications. *MedChemComm* **2010**, *1*, 183−198.

(29) Hall, D. G. Structure, properties, and preparation of boronic acid derivatives overview of their reactions and applications, in boronic acids: preparation and applications in organic synthesis and medicine. In *Boronic Acids Preparations and Applications in Organic Synthesis and Medicine*; Hall, D. G., Ed.; Wiley-VCH Verlag GmbH & Co. KGaA: Weinheim, 2006; pp 1−99.

(30) Roy, C. D.; Brown, H. C. Stability of boronic esters—structural effects on the relative rates of transesterification of 2-(phenyl)-1,3,2-dioxaborolane. *J. Organomet. Chem.* **2007**, *692*, 784−790.

(31) Roy, C. D.; Brown, H. C. A comparative study of the relative stability of representative chiral and achiral boronic esters employing transesterification. *Monatsh. Chem.* **2007**, *138*, 879−887.

(32) Roush, W. R.; Walts, A. E.; Hoong, L. K. Diastereoselective and enantioselective aldehyde addition-reactions of 2-allyl-1,3,2-dioxaborolane-4,5-dicarboxylic esters, a useful class of tartrate ester modified allylboronates. *J. Am. Chem. Soc.* **1985**, *107*, 8186−8190.

(33) Bernardini, R.; Oliva, A.; Paganelli, A.; Menta, E.; Grugni, M.; De Munari, S.; Goldoni, L. Stability of boronic esters to hydrolysis: a comparative study. *Chem. Lett.* **2009**, *38*, 750−751.

(34) Yan, J.; Springsteen, G.; Deeter, S.; Skeuse, C.; Wang, B. H. The relationship among pK_a, pH, and binding constants in the interactions between boronic acids and diols—it is not as simple as it appears. *Tetrahedron* **2004**, *60*, 11205−11209.

(35) Aznar, E.; Dolores Marcos, M.; Martinez-Manez, R.; Sancenon, F.; Soto, J.; Amoros, P.; Guillem, C. pH- and photo-switched release of

guest molecules from mesoporous silica supports. *J. Am. Chem. Soc.* **2009**, *131*, 6833−6843.
(36) Springsteen, G.; Wang, B. H. A detailed examination of boronic acid-diol complexation. *Tetrahedron* **2002**, *58*, 5291−5300.
(37) Gillis, E. P.; Burke, M. D. A simple and modular strategy for small molecule synthesis: iterative Suzuki−Miyaura coupling of B-protected haloboronic acid building blocks. *J. Am. Chem. Soc.* **2007**, *129*, 6716−+.
(38) Knapp, D. M.; Gillis, E. P.; Burke, M. D. A general solution for unstable boronic acids: slow-release cross-coupling from air-stable MIDA boronates. *J. Am. Chem. Soc.* **2009**, *131*, 6961−+.
(39) Stolowitz, M. L.; Ahlem, C.; Hughes, K. A.; Kaiser, R. J.; Kesicki, E. A.; Li, G. S.; Lund, K. P.; Torkelson, S. M.; Wiley, J. P. Phenylboronic acid−salicylhydroxamic acid biconjugates. 1. A novel boronic acid complex for protein immobilization. *Bioconjugate Chem.* **2001**, *12*, 229−239.
(40) Wiley, J. P.; Hughes, K. A.; Kaiser, R. J.; Kesicki, E. A.; Lund, K. P.; Stolowitz, M. L. Phenylboronic acid−salicylhydroxamic acid bioconjugates. 2. Polyvalent immobilization of protein ligands for affinity chromatography. *Bioconjugate Chem.* **2001**, *12*, 240−250.
(41) Greige-Gerges, H.; Diab, Y.; Farah, J.; Magdalou, J.; Haddad, C.; Ouaini, N. Ferutinin stability in human plasma and interaction with human serum albumin. *Biopharm. Drug Dispos.* **2008**, *29*, 83−89.
(42) Tirosh, O.; Barenholz, Y.; Katzhendler, J.; Priev, A. Hydration of polyethylene glycol-grafted liposomes. *Biophys. J.* **1998**, *74*, 1371−1379.
(43) Barenholz, Y. Liposome application: problems and prospects. *Curr. Opin. Colloid Interface Sci.* **2001**, *6*, 66−77.
(44) Stefanick, J. F.; Ashley, J. D.; Kiziltepe, T.; Bilgicer, B. A systematic analysis of peptide linker length and liposomal polyethylene glycol coating on cellular uptake of peptide-targeted liposomes. *ACS Nano* **2013**, *7* (4), 2935−2947.
(45) Stefanick, J. F.; Ashley, J. D.; Bilgicer, B. Enhanced cellular uptake of peptide-targeted nanoparticles through increased peptide hydrophilicity and optimized ethylene glycol peptide-linker length. *ACS Nano* **2013**, *7* (9), 8115−8127.